Biomedicine & Pharmacotherapy 156 (2022) 113754

Contents lists available at ScienceDirect

Biomedicine & Pharmacotherapy

journal homepage: www.elsevier.com/locate/biopha

Flavonoids from *Ericameria nauseosa* inhibiting PI3K/AKT pathway in human melanoma cells

Tanja Hell [a], Maciej Dobrzyński [b], Fabian Gröflin [a], Jakob K. Reinhardt [a], Lara Dürr [a], Olivier Pertz [b], Matthias Hamburger [a], Eliane Garo [a,*]

[a] Division of Pharmaceutical Biology, Department of Pharmaceutical Sciences, University of Basel, Basel, Switzerland
[b] Institute of Cell Biology, University of Bern, Baltzerstrasse 4, 3012 Bern, Switzerland

ARTICLE INFO

Keywords:
Ericameria nauseosa
Melanoma
PI3K/AKT
MAPK/ERK
HPLC-based activity profiling
Flavonoids

ABSTRACT

The PI3K/AKT and MAPK/ERK pathways are frequently mutated in metastatic melanoma. In a screen of over 2500 plant extracts, the dichloromethane extract of *Ericameria nauseosa* significantly inhibited oncogenic activity of AKT in MM121224 human melanoma cells. This extract was analyzed by analytical HPLC, and the column effluent was fractionated and tested for activity to generate the so-called HPLC-based activity profile. Compounds eluting within active time-windows of the chromatogram were subsequently isolated in a larger scale to afford 11 flavones (**1**-**11**), four flavanones (**12**-**15**), two diterpenes (**16**, **17**), and a seco-caryophyllene (**18**). All isolated compounds were tested for activity, whereby only flavonoids were found active. Of these, flavones were shown to be more active than the flavanones. The most potent flavone was compound **9**, that was displaying an IC_{50} of 14.7 ± 1.4 μM on AKT activity in MM121224 cells. The terpenoids (**16**-**18**) were found to be inactive in the assay. Both diterpenes, a grindelic acid derivative (**16**) and an *ent*-neo-clerodane (**17**) were identified as new natural products. Their absolute configuration was established by ECD. Compound **17** is the first description of a clerodane type diterpene in the genus *Ericameria*.

1. Introduction

Malignant melanoma is the most lethal dermatological cancer, and its incidence has increased rapidly over the last decades [1]. Various driver mutations have been identified in melanoma cells, in particular in the MAPK/ERK (mitogen-activated protein kinase/extracellular signal-regulated kinase) and the PI3K/AKT (phosphoinositide 3-kinase/AK strain transforming kinase) pathways [2]. The *BRAF* (v-raf murine sarcoma viral oncogene homolog B1) V600 is the most prominent mutation occurring in 50–70% of all melanoma [3,4], and mutations in *NRAS* are found in 15–20% of melanoma. The PI3K pathway is estimated to be affected in 15% of cases [5]. Given that the two pathways are critically involved in cell growth and proliferation, such mutations contribute to uncontrolled pathway signaling and, therefore, to cancer progression.

Drugs specifically targeting mutated BRAF V600, such as vemurafenib, dabrafenib, and encorafenib have been developed. Initial clinical results with vemurafenib and dabrafenib were very promising, however, patients relapsed after only 5–7 months of treatment due to drug resistance [6,7]. The combination of two MAPK/ERK pathway inhibitors, namely a BRAF and a MEK inhibitor, has been recently shown to improve survival, progression-free survival, and overall response rate [8]. Nevertheless, the 5-year relative survival rate for advanced metastatic melanoma is still only 29.8% [9]. A rational therapeutic option is to simultaneously target the PI3K/AKT and MAPK/ERK pathways. Therefore, new inhibitors targeting one or both of these pathways are urgently needed.

We recently developed a high-content screening (HCS) pipeline to screen for MAPK/ERK and PI3K/AKT pathway inhibitors in two human melanoma cell lines, namely the well-established A2058 and the patient-derived MM121224 cells [10]. The A2058 cell line is bearing a *BRAF* V600E mutation and a *PTEN* deletion, while the MM121224 cell line bears a *BRAF* V600E mutation, and an *NRAS* Q61K mutation acquired after vemurafenib treatment [11]. The *BRAF* V600E mutation leads to increased MAPK/ERK activity, and the *PTEN* deletion to increased PI3K activity. The *NRAS* Q61K mutation results in Ras-dependent PI3K activation and, as a consequence, to increased PI3K/AKT pathway activity. These cell lines were designed to express genetically encoded kinase

* Corresponding author.
E-mail address: eliane.garo@unibas.ch (E. Garo).

https://doi.org/10.1016/j.biopha.2022.113754
Received 12 September 2022; Accepted 26 September 2022
Available online 17 October 2022

translocation reporters (KTR) that report simultaneously on ERK and AKT kinase activity in individual cells [10,12]. A KTR biosensor consists of the kinase substrate binding site, a fluorescent protein for detection, and a domain that converts phosphorylation/dephosphorylation into a nuclear-cytosolic shuttling effect [12]. Thus, when a pathway is inactive (e.g. in the presence of an inhibitor), its biosensor is located in the nucleus, whereas when its activity is high, the KTR biosensor gets phosphorylated and shuttles into the cytosol. This read-out enables to simultaneously screen for MAPK/ERK and PI3K/AKT pathways inhibitors.

A library of more than 2500 plant extracts was recently screened with this assay to search for new compounds inhibiting oncogenic ERK and AKT activities [10]. The dichloromethane (DCM) extract of *Ericameria nauseosa* (Pall. ex Pursh) G.L. Nesom & G.I. Baird (*Chrysothamnus nauseosus* (Pall. ex Pursh) Britt.) [13,14] was found to significantly inhibit AKT activity in MM121224 cells [10]. *E. nauseosa* is a shrub widely occurring in arid regions of western North America [15]. Interestingly, a wide range of natural products scaffolds, such as flavonoids, monoterpenes, sesquiterpenes, labdane diterpenes, and polyacetylenes have been reported previously in *E. nauseosa* [16–19].

The HPLC-based activity profiling strategy [20] was applied to this extract. Compounds eluting in active time-windows were pinpointed as being potentially responsible for the activity of the extract. We herein report on the targeted isolation of all these compounds, and on their activity on AKT and ERK signaling in both MM121224 and A2058 cells.

2. Materials and methods

2.1. General

HPLC-grade MeOH, MeCN, formic acid (FA) and dimethyl sulfoxide (DMSO) were obtained from Scharlau or Macron Fine Chemicals. Ultrapure water from a Milli-Q water purification system (Merck Millipore) was used for HPLC separations. Solvents used for extraction, column chromatography and TLC were of technical grade and were redistilled before use. Reference substances of apigenin (ALEXIS Biochemicals/Enzo Life Sciences), kaempferol, quercetin (both Sigma-Aldrich/Merck), luteolin (AdipoGen), hesperetin, isoquercetin (both Roth) were used.

Normal-phase flash chromatography was carried out on a Puriflash 4100 system (Interchim) consisting of a pump, a PDA detector, and a fraction collector. A glass column (46 × 7 cm i.d.) was packed with Silica gel 60 (15–40 μm to pack column; 40–63 μm for dry load of sample) from Merck. TLC plates (Silca gel 60 F254, Merck) were visualized under UV light and by spraying with 1% vanillin (Roth) in EtOH, followed by 10% sulfuric acid (Scharlau) in EtOH and heating at 110 °C.

Gel chromatography was carried out on a Sephadex LH-20 column (93 × 2.7 cm i.d.) (Sigma Aldrich/Merck) connected to a Kappa Isocratic pump (ECOM) and a C-660 fraction collector (Büchi). The column was eluted with 100% MeOH at a flow rate of 0.6–2.7 mL/min.

Preparative HPLC separations were performed on a 1290 Infinity II Preparative LC/MS system (Agilent Technologies) consisting of a binary pump and an Agilent 1100 PDA detector in line with an Agilent 6120 Quadrupole LC/MS detector. The column effluent was collected via a split (100:1) between HPLC column and detectors. A SunFire Prep C18 OBD column (5 μm, 150 ×30 mm, Waters) equipped with a C18 Prep guard column (10 × 30 mm) was used at a flow rate of 20 mL/min.

Semi-preparative HPLC was carried out on a HP 1100 Series system (Agilent Technologies) consisting of a binary pump, auto-sampler and a PDA. If not mentioned otherwise, separations were carried out with a SunFire Prep C18 column (5 μm, 150 × 10 mm, Waters) equipped with a guard column (10 × 10 mm) at a flow rate of 4 mL/min.

HPLC-PDA-ELSD-ESIMS analysis was performed on a LC-MS 8030 system (Shimadzu) consisting of degasser, binary high-pressure mixing pump, auto-sampler, column oven, and PDA detector. A triple quadrupole MS (LCMS-8030, Shimadzu) and an ELSD 3300 detector (Alltech) were connected via a T-splitter (1:10) to the system. A SunFire C18 column (3.5 μm, 150 × 3 mm, Waters) equipped with a C18 guard column (10 × 3 mm) was used at a flow rate of 0.4 mL/min.

NMR spectra were recorded on a Bruker Avance III NMR spectrometer operating at 500.13 MHz for ^{1}H and 125.77 MHz for ^{13}C nuclei, equipped with a 5 mm BBO probe operated at 23 °C. Spectra were recorded in $CDCl_3$ (Sigma-Aldrich/Merck) or DMSO-d_6 (Armar Chemicals), and analyzed using Bruker TopSpin 3.5 and ACD/Labs NMR Workbook suites software. Chemical shifts are reported as δ values (ppm), with residual signal as internal reference, J in Hz.

Optical rotations were measured in MeOH on a P-2000 digital polarimeter (Jasco) equipped with a sodium lamp (589 nm) and a 10 cm temperature-controlled microcell. UV and ECD spectra were recorded in MeOH (0.17–1.3 mM) on a Chirascan CD spectrometer using 1 mm path precision cells (110 QS, Hellma Analytics). HRESIMS data were measured on an LQT XL Orbitrap mass spectrometer (Thermo Scientific).

2.2. Plant material

Aerial parts of *Ericameria nauseosa* (Pall. ex Pursh) G.L. Nesom & G.I. Baird (syn. *Chrysothamnus nauseosus* (Pall. ex Pursh) Britt.) were collected and identified by Matthias Hamburger on 12.08.1999 in Pinyon-Juniper-Woodland (1500–1700 m above sea level, east entry of Arizona State Route 89, near Yarnell AZ, USA). A voucher specimen has been deposited at the Division of Pharmaceutical Biology, University of Basel, under plant number 23.

2.3. HPLC-based activity profiling

The in-house library extract of *E. nauseosa* (10 mg/mL DMSO) was microfractionated on an analytical HPLC system (Shimadzu) connected to an FC 204 fraction collector (Gilson) adapted for 96-deepwell plates. Three injections of the extract were carried out: 2 × 30 μL (corresponding to 600 μg of extract) with only the PDA detector for microfractionation, and 1 × 10 μL with PDA-ELSD-ESIMS detection for on-line spectroscopic analysis and to generate the HPLC-based activity profile. Water with 0.1% FA (A) and MeCN with 0.1% FA (B) were used as mobile phase. The following elution profile was used: 10% B for 3 min, followed by a linear gradient to 100% B in 27 min, and 10 min at 100% B. 24 microfractions of 1.5 min each were collected from min 2 to min 38, whereby corresponding microfractions of the two runs were collected into the same well of a 96-deepwell plate. The plate was dried in a Genevac EZ-2 evaporator.

2.4. Extraction and isolation

Dried herb of *E. nauseosa* (83 g) was frozen with liquid nitrogen and ground with a Retsch GM 200 mill. The ground material was macerated under stirring at r.t. with CH_2Cl_2 (9 × 500 mL, 8–24 h each). The solvent was evaporated at reduced pressure to yield 10.3 g of dry extract which was stored at 4 °C.

The extract was separated by flash chromatography on silica gel by using a gradient of $CHCl_3$ (A) and 40% MeOH in $CHCl_3$ (B) at a flow rate of 25 mL/min. The sample was introduced as dry load (10 g extract adsorbed to 30 g silica gel). The following gradient was used: 0% B (0–10 min); 0% → 12% B (10–70 min); 12% → 25% B (70–130 min); 25% B (130–160 min); 25% → 40% B (160–190 min); 40% → 75% B (190–220 min); 75% → 100% B (220–230 min); 100% B (230–275 min). The column was further washed with B and MeOH (C): 0% → 100% C (275–305 min); 100% C (305–410 min). Fractions collected (22 mL each) were pooled to 12 main fractions (A-L) based on their TLC pattern (MeOH/$CHCl_3$ 10:90).

Fractions D (527 mg) and H (1580 mg) were submitted to preparative RP-HPLC [H_2O (A), MeCN (B); 30–90% B, and 30–70%, respectively (0–30 min)]. Fraction D afforded **8** (11.1 mg, t_R 17.0 min) and **15** (44.2

mg, t_R 18.4 min). Fraction H afforded two main fractions H1 (80.1 mg) and H5 (53.0 mg). Fraction H1 was separated with semi-preparative HPLC [H_2O (A), MeCN (B); 18% B.), Xbridge Prep C18 (5 μm, 150 × 10 mm; guard column 5 μm, 10 × 10 mm, Waters)] to afford **2** (26.2 mg, t_R 17.9 min) and sub-fraction H1b (17.1 mg). H1b afforded **1** (10.5 mg, t_R 23.0 min) by using 45% MeOH at a flow rate of 3.5 mL/min. Semi-preparative HPLC of fraction H5 [H_2O + 0.1% FA (A), MeCN + 0.1% FA (B); 40–43% B (0–20 min)] afforded **16** (9.4 mg, t_R 14.0 min), **18** (6.7 mg, t_R 15.7 min) and **17** (11.9 mg, t_R 16.5 min).

Fractions E (1.4 g), F (0.5 g) and G (1.7 g) were individually separated on a Sephadex LH-20 column. Fractions [12 min (F); 10 min (E, G)] collected were pooled according to TLC patterns (EtOAc/Hexane 70:30). Fraction E afforded E1-E6, fraction F gave F1-F10, and fraction G afforded fractions G1-G6. Compound **6** (14.3 mg) was obtained from fraction F9. The following fractions were submitted to semi-preparative RP-HPLC using H_2O + 0.1% FA (A) and MeCN + 0.1% FA (B) as mobile phase. Fraction E4 (31.5 mg) was separated with a gradient of 25–55% B in 30 min to obtain **13** (3.2 mg, t_R 16.0 min), **11** (2.0 mg, t_R 27.7 min) and E4f (6.4 mg). Separation of fraction E4f with 47% B afforded **14** (5.5 mg, t_R 12.0 min). Fraction E5 (92.8 mg) was separated with a gradient of 30–50% B in 30 min to afford **12** (4.1 mg, t_R 14.0 min) and **9** (7.6 mg, t_R 28.9 min). Fraction E6 (15.7 mg) was separated with a gradient of 30–50% B in 30 min to afford **10** (1.1 mg, t_R 25.6 min) and E6b (2.4 mg). Fraction E6b was separated with 32% B to yield **7** (1.2 mg, t_R 35.4 min). Fraction G6 (12.7 mg) was separated using 30–40% B in 30 min to afford **3** (2.0 mg, t_R 16.6 min). Fraction F8 was separated by semi-preparative HPLC using two different methods both on a Reprosil-Pur 120 C18-AQ column (3 μm, 10 × 150 mm, Dr. Maisch). The first method consisted of 50% MeOH + 0.1% FA to afford **4** (1.4 mg, t_R 50.0 min) and **5** (2.0 mg, t_R 53.5 min). A second method using 50% MeCN + 0.1% FA at a flow rate of 3.5 mL/min afforded **5** (1.5 mg, t_R 12.6 min). Compound **5** had a purity of ~80%.

7,4'-Dihydroxy-3,5,8,3'-trimethoxyflavone (**1**): pale yellow amorphous powder; ^{1}H and ^{13}C NMR, see Table S1, Supporting Information; HRESIMS *m/z* 375.1076 $[M+H]^+$ (calcd for $C_{19}H_{19}O_8^+$, 375.1074).

7,4'-Dihydroxy-3,5,8-trimethoxyflavone (**2**): white powder; ^{1}H and ^{13}C NMR, see Table S1, Supporting Information; HRESIMS *m/z* 345.0974 $[M+H]^+$ (calcd for $C_{18}H_{17}O_7^+$, 345.0969).

Isorhamnetin (**3**): yellow amorphous powder; ^{1}H and ^{13}C NMR, see Table S1, Supporting Information; HRESIMS *m/z* 317.0658 $[M+H]^+$ (calcd for $C_{16}H_{13}O_7^+$, 317.0656).

5,7,3'-Trihydroxy-3,8,4'-trimethoxyflavone (**4**): yellow amorphous powder; ^{1}H and ^{13}C NMR, see Table S2, Supporting Information; HRESIMS *m/z* 361.0919 $[M+H]^+$ (calcd for $C_{18}H_{17}O_8^+$, 361.0918).

5,7,4'-Trihydroxy-3,8,3'-trimethoxyflavone (**5**): yellow oily residue; ^{1}H and ^{13}C NMR, see Table S2, Supporting Information; HRESIMS *m/z* 361.0919 $[M+H]^+$ (calcd for $C_{18}H_{17}O_8^+$, 361.0918).

5,7,4'-Trihydroxy-3,3'-dimethoxyflavone (**6**): yellow amorphous powder; ^{1}H and ^{13}C NMR, see Table S2, Supporting Information; HRESIMS *m/z* 331.0813 $[M+H]^+$ (calcd for $C_{17}H_{15}O_7^+$, 331.0812).

3,5,7-Trihydroxy-3',4'-dimethoxyflavone (**7**): yellow amorphous powder; ^{1}H and ^{13}C NMR, see Table S3, Supporting Information; HRESIMS *m/z* 331.0811 $[M+H]^+$ (calcd for $C_{17}H_{15}O_7^+$, 331.0812).

5,7-Dihydroxy-3,8,3',4'-tetramethoxyflavone (**8**): yellow amorphous powder; ^{1}H and ^{13}C NMR, see Table S3, Supporting Information; HRESIMS *m/z* 375.1076 $[M+H]^+$ (calcd for $C_{17}H_{15}O_7^+$, 375.1074).

5,7-Dihydroxy-3,3',4'-trimethoxyflavone (**9**): yellow amorphous powder; ^{1}H and ^{13}C NMR, see Table S3, Supporting Information; HRESIMS *m/z* 345.0972 $[M+H]^+$ (calcd for $C_{18}H_{17}O_7^+$, 345.0969).

Galangin (**10**): yellow amorphous powder; ^{1}H and ^{13}C NMR, see Table S4, Supporting Information; HRESIMS *m/z* 271.0601 $[M+H]^+$ (calcd for $C_{15}H_{11}O_5^+$, 271.0601).

5,7-Dihydroxy-3-methoxyflavone (**11**): orange amorphous powder; ^{1}H and ^{13}C NMR, see Table S4, Supporting Information; HRESIMS *m/z* 285.0762 $[M+H]^+$ (calcd for $C_{16}H_{13}O_5^+$, 285.0757).

(2*R*,3*R*)-*3',4'-O-Dimethyltaxifolin* (**12**): yellow amorphous powder; $[\alpha]_D^{25} = -51.1$ (*c* 0.25, MeOH); UV (MeOH) λ_{max} (log ε) 200 (4.5), 230 (4.1, sh), 289 (4.4) nm; 311 (3.4, sh) nm ECD (*c* 0.17 mM mg/mL, MEOH) λ_{max} (Δε) 200 nm (+9.0), 210 nm (−6.8), 221 nm (+10.4), 293 nm (−10.4), 329 nm (+2.6); ^{1}H and ^{13}C NMR, see Table S5, Supporting Information; HRESIMS *m/z* 333.0969 $[M+H]^+$ (calcd for $C_{17}H_{17}O_7^+$, 333.0969).

Pinobanksin (**13**): yellow oily residue; $[\alpha]_D^{25} = -9.2$ (*c* 0.10, MeOH); UV (MeOH) λ_{max} (log ε) 212 (4.3, sh), 292 (4.1), 334 (3.5, sh) nm; ECD (*c* 0.41 mM, MeOH) λ_{max} (Δε) 222 nm (+11.9), 290 nm (−6.6), 329 nm (+2.5); ^{1}H and ^{13}C NMR, see Table S5, Supporting Information; HRESIMS *m/z* 273.0758 $[M+H]^+$ (calcd for $C_{15}H_{13}O_5^+$, 273.0757).

Pinobanksin-3-acetate (**14**): orange amorphous powder; $[\alpha]_D^{25} = 28.7$ (*c* 0.10, MeOH); UV (MeOH) λ_{max} (log ε) 211 (4.4), 293 (4.2), 334 (3.6, sh) nm; ECD (*c* 0.35 mM, MeOH) λ_{max} (Δε) 221 (+16.5), 288 (−9.4), 323 (+2.9); ^{1}H and ^{13}C NMR, see Table S5, Supporting Information; HRESIMS *m/z* 315.0865 $[M+H]^+$ (calcd for $C_{17}H_{15}O_6^+$, 315.0863).

Pinocembrin (**15**): pale yellow powder; $[\alpha]_D^{25} = -54.7$ (*c* 0.10, MeOH); UV (MeOH) λ_{max} (log ε) 211 (4.5), 289 (4.2), 331 (3.6, sh) nm; ECD (*c* 0.32 mM, MeOH) λ_{max} (Δε) 219 nm (+22.8), 286 nm (−14.5), 324 nm (+3.9); ^{1}H and ^{13}C NMR, see Table S4, Supporting Information; HRESIMS *m/z* 257.0807 $[M+H]^+$ (calcd for $C_{15}H_{13}O_4^+$, 257.0808).

(2*S*,5*S*,9*R*,10*S*,13*S*)-*2-Hydroxygrindelic acid* (**16**): clear oil; $[\alpha]_D^{25} = -124.6$ (*c* 0.09, MeOH); UV (MeOH) λ_{max} (log ε) 195 (3.9); ECD (*c* 0.99 mM, MeOH) λ_{max} (Δε) 199 nm (−14.2); ^{1}H and ^{13}C NMR, see Table S6, Supporting Information; HRESIMS *m/z* 337.2375 $[M+H]^+$ (calcd for $C_{20}H_{33}O_4^+$, 337.2373).

(2R,5R,8S,9R,10S,13)-2-Hydroxy-clerod-3-en-18-al-15-oic acid* (**17**): pale yellow oil; $[\alpha]_D^{25} = 36.6$ (*c* 0.09, MeOH); UV (MeOH) λ_{max} (log ε) 236 (3.8); ECD (*c* 0.99 mM, MeOH) λ_{max} (Δε) 210 nm (−8.4), 243 (+10.0); ^{1}H and ^{13}C NMR, see Table S6, Supporting Information; HRESIMS *m/z* 337.2372 $[M+H]^+$ (calcd for $C_{18}H_{17}O_7^+$, 337.2373).

(1*R*,4*,9*S*)-*4-Hydroxy-4,5-seco-caryophyllen-5-oic acid* (**18**): clear oil; $[\alpha]_D^{25} = 58.6$ (*c* 0.09, MeOH); UV (MeOH) λ_{max} (log ε) 195 (3.9); ECD (*c* 1.31 mM, MeOH) λ_{max} (Δε): 219 nm (−0.2), 241 (+0.2); ^{1}H and ^{13}C NMR, see Table S6, Supporting Information; HRESIMS *m/z* 255.1955 $[M+H]^+$ (calcd for $C_{15}H_{27}O_3^+$, 255.1955).

2.5. Testing of bioactivity

Bioactivity was measured using a high-content assay recently developed in our lab [10]. In brief, A2058 (ATTC-CRL-11147) and MM121224 [11] wild type (WT) cells were transfected to genetically encode ERK- and AKT-KTRs. For the experiments, cells were seeded in 96-well plates and incubated with the samples (fractions, crude extract of *E. nauseosa*, or pure compounds). Afterward, cells were fixed and imaged with a high-content screening (HCS) microscope. A computer vision approach was used to automatically segment each cell and extract a ratio of fluorescence intensity in cytosol over nucleus as a measure of ERK or AKT activity. Results were displayed as normalized percentage inhibition (NPI). Positive controls for the A2058 cells were 20 μM AZD5363 (Selleckchem) as AKT inhibitor, and 500 nM cobimetinib (Selleckchem) as ERK pathway inhibitor. For the MM121224 cells, 1 μM GDC0941 (Selleckchem) as PI3K/AKT pathway inhibitor, and 200 nM cobimetinib as MAPK/ERK pathway inhibitor were used. The negative control was 0.75% DMSO in complete medium. The compounds were tested in triplicate at eight different concentrations ranging from 200 μM to 1.56 μM. Immunostaining was performed as recently reported [10].

2.6. In silico predictions

Physicochemical and ADME properties for all isolated compounds were calculated on the ACD/Percepta platform (ACD/Labs, 2020.1.1).

ECD spectra were calculated in the following fashion. The initial

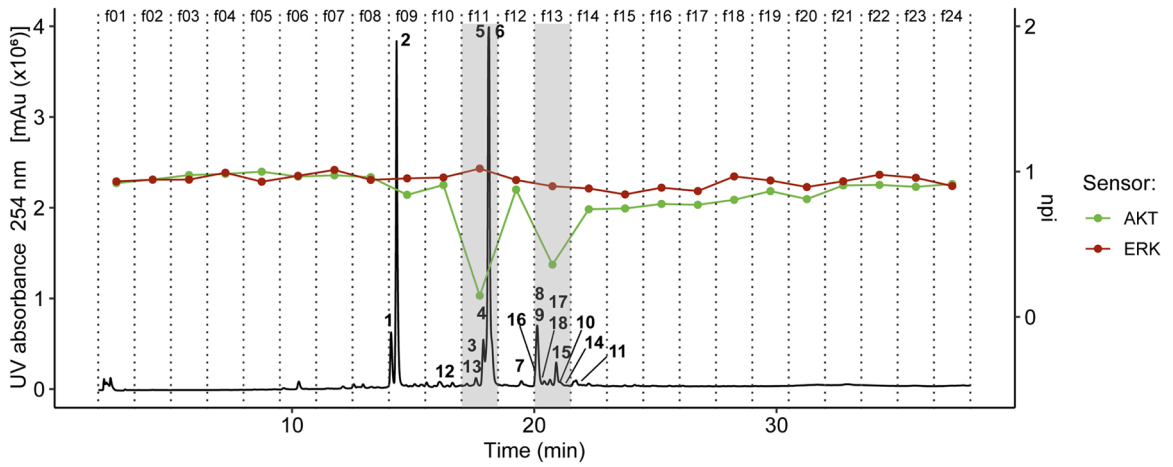

Fig. 1. HPLC-based activity profile of the dichloromethane extract of *E. nauseosa*. The HPLC-UV chromatogram at 254 nm is shown from min 2–38. Microfractions collected are indicated by dotted lines. The activity of AKT (green line) and ERK (red line) in MM121224 cells is reported as the normalized percentage of inhibition (NPI). Bold numbers refer to isolated compounds **1**-**18**. (For interpretation of the references to colour in this figure legend, the reader is referred to the web version of this article.)

conformational analysis was performed with MacroModel (Schrödinger Release 2020–2, LLC, New York) in two-steps, both employing the OPLS2005 (optimized potential for liquid simulations) force field in H_2O. First, the global minimum of the input structure was searched over 30,000 steps, which was then used as the input for a conformational search over 10,000 steps to find the six conformers with the lowest energies (20 in case of compound **18** due to its flexibility). The resulting conformers were used as the starting point for quantum mechanical calculations. Initially, the geometry was optimized and the energy calculated by applying DFT at the CAM-B3LYP/Def2SVP level of theory, and employing the SCRF method and the CPMC model for solvation in MeOH with the Gaussian 09 program package [21]. Then, excitation energy (denoted by wavelength in nm), rotator strength (R_{str}), dipole velocity (R_{vel}), and dipole length (R_{len}) were calculated in MeOH by TD-DFT at the same level of theory. The depicted ECD curves were obtained on the basis of rotator strengths with a half-band of 0.25 eV and a shift of the spectrum by + 10 nm using SpecDis v1.71 [22].

3. Results and discussion

3.1. HPLC-based activity profiling and identification of compounds

The DCM extract of *E. nauseosa* was recently identified as a hit in a HCS of 2576 plant extracts for MAPK/ERK and PI3K/AKT pathway inhibitors in melanoma cells [10]. This extract, tested at a concentration of 75 μg/mL in MM121224 cells, was shown to inhibit AKT activity with an NPI value of 0.32. The extract was then analyzed by HPLC-based activity profiling [20]. Thus, a total of 600 μg of extract was separated by analytical HPLC and fractions collected in a 96-deepwell plate for activity testing. The UV, MS and ELSD data were recorded in parallel. The overlay of the HPLC chromatogram with the bioactivity data provided the so-called HPLC-based activity profile (Fig. 1) [20]. Microfractions 11 and 13 both strongly inhibited the AKT activity (NPI values of 0.17 and 0.39, respectively), whereas ERK activity was not affected by any of the fractions (Fig. 1). Compounds eluting in these active fractions were targeted by preparative isolation.

A scale-up extract of *E. nauseosa* was prepared from a larger portion (83 g) of plant material. The extract was subjected to a combination of different chromatographic methods, including flash chromatography on silica gel, gel chromatography, and preparative and semi-preparative RP-HPLC to afford a total of 18 compounds (Fig. 2 and 3), 14 of which were eluting in one of the two active time windows of the activity profile. The minor compounds **7** and **12** were also obtained during this isolation process. Compounds **1** and **2** corresponding to the two major UV absorbing peaks outside of the active time windows were also isolated Fig. 1.

The UV spectra of compounds **1**-**11** exhibited UV spectra typical for flavones, with two major absorption maxima in the regions of 250–272 nm and 310–370 nm [23]. Compounds **12**-**15** had absorption maxima at 288-294 nm with a broad shoulder at 320–360 nm, suggesting the presence of flavanones/flavanols [23]. In contrast, compounds **16**-**18** showed only one absorption maximum in the region of 200–233 nm.

Compounds **12**-**15** displayed signals of aliphatic protons between δ_H 2.78–5.93, and carbons between δ_C 42.1–83.0 ppm, typical for flavanones [23]. In contrast, the chemical shifts of C-2 of **1**-**11** appeared in the downfield region between δ_C 145.5–155.5 ppm, confirming the presence of flavones.

In the ^{1}H NMR spectra of compounds **1**-**15**, resonances for aromatic protons of ring A (δ_H 5.86–6.48) and ring B (δ_H 6.94–8.16) were observed. In addition, the spectra of compounds **1**, **3**-**9**, and **12** showed signals of an ABX system between δ_H 6.94 and 7.80, for the protons in the ring B. The ^{1}H NMR data of compound **2** showed a typical A_2B_2 pattern (H-2′/H-6′ and H-3′/H-5′, δ_H 7.92 and 6.95). Compounds **10**, **11,** and **13**-**15** all showed resonances of five protons between δ_H 7.39–8.16, thereby suggesting that ring B was not substituted. Most of the flavonoids (**1**-**9**, **11, 12**) were methoxylated, as suggested by the presence of singlets at δ_H 3.72-3.86 integrating for three protons each.

The relative configuration of flavanonols **12**-**14** was determined based on the vicinal coupling constant $J_{2,3} > 11$ Hz indicative of a *trans* position. Complete NMR spectral assignments were achieved by 1D and 2D NMR, and the absolute configuration of flavanones was established by ECD. The experimental spectra of compounds **12–14** showed a negative cotton effect at 290 nm and a positive cotton effect at 330 nm. This was in line with calculated spectra for the (2*R*,3*R*) configuration (S1, Supporting Information). Flavanone **15** was established in comparison with the calculated spectra to have a 2 *S* configuration (S1, Supporting Information). The flavonoids were thus identified as 7,4'-dihydroxy-3,5,8,3'-tetramethoxyflavone (**1**) [24,25], 7,4'-dihydroxy-3,5,8-trimethoxyflavone (**2**) [26], isorhamnetin (**3**) [27], 5,7,3'-trihydroxy-3,8,4'-trimethoxyflavone (**4**) [28,29], 5,7,4'-trihydroxy-3,8,3'-trimethoxyflavone (**5**) [30], 5,7,4'-trihydroxy-3',4'-dimethoxyflavone (**6**) [31], 3,5,7-trihydroxy-3',4'-dimethoxyflavone (**7**) [32], 5,7-dihydroxy-3,8,3',4'-tetramethoxyflavone (**8**) [30], 5,7-dihydroxy-3,3',4'-trimethoxyflavone (**9**) [33], galangin (**10**) [34], 5,7-dihydroxy-3-methoxyflavone (**11**) [35], (2*R*,3*R*)-3',4'-O-dimethyltaxifolin (**12**) [36,37], pinobanksin (**13**) [34],

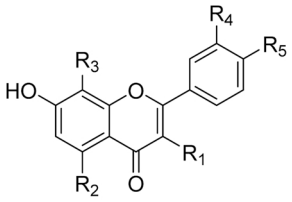

Compound	R_1	R_2	R_3	R_4	R_5
1	OCH_3	OCH_3	OCH_3	OCH_3	OH
2	OCH_3	OCH_3	OCH_3	H	OH
3	OH	OH	H	OCH_3	OH
4	OCH_3	OH	OCH_3	OH	OCH_3
5	OCH_3	OH	OCH_3	OCH_3	OH
6	OCH_3	OH	H	OCH_3	OH
7	OH	OH	H	OCH_3	OCH_3
8	OCH_3	OH	OCH_3	OCH_3	OCH_3
9	OCH_3	OH	H	OCH_3	OCH_3
10	OH	OH	H	H	H
11	OCH_3	OH	H	H	H

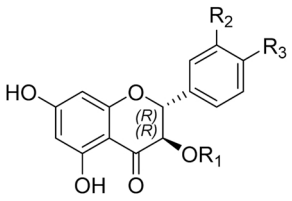

Compound	R_1	R_2	R_3
12	H	OCH_3	OCH_3
13	H	H	H
14	$COCH_3$	H	H

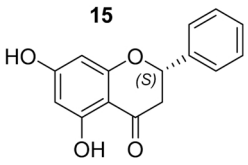

Fig. 2. Flavonoids isolated from the dichloromethane extract.

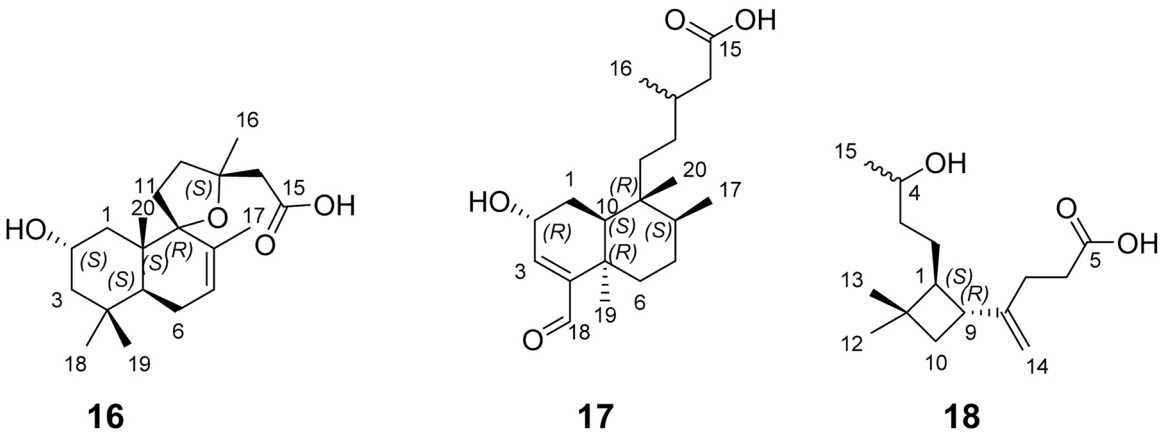

Fig. 3. Structures of diterpenes **16** and **17**, and sesquiterpene **18**.

pinobanksin-3-acetate (**14**) [35], and (2*S*)-pinocembrin (**15**) [38,39]. The flavonoids **3**, **6**, **9** and **15** have been described previously from *E. nauseosa* [17,40], whereas **1**, **4**, **5**, **7**, **8** and **10**-**14** are new to the genus *Ericameria*. Flavonol **2** has been previously reported as a synthetic compound but, to our knowledge, not as a naturally occurring compound Fig. 2.

Compound **16** was analyzed by HRESIMS (*m/z* 337.2375 $[M+H]^+$, calcd. for $C_{20}H_{32}O_4^+$, 337.2373) and NMR for $C_{20}H_{32}O_4$, a formula requiring five degrees of unsaturation. The NMR data revealed the presence of three sp^2 carbons (one carbonyl and two olefinic carbons) and thus suggested a tricyclic ring system. The ^1H NMR spectrum showed resonances attributed to one olefinic proton (δ_H 5.64), two methine (δ_H 1.61, 3.91), six non-equivalent methylene (δ_H 1.50/1.81, 1.18/1.78, 1.85/2.11, 1.99/2.17, 2.00/2.07, 2.59/2.71), and five methyl groups (δ_H 0.88, 0.95, 0.96, 1.41, 1.79). The ^{13}C NMR data in addition revealed the presence of a carboxylic acid moiety (δ_C 171.5). In the HMBC spectrum crosspeaks were observed from H_3-17 to C-7, C-8 and C-9, from H_3-20 to C-9 and C-10, as well as from H_3-18 and H_3-19 to C-3, C-4 and C-5. From these data, the scaffold of **16** was identified as a labdane diterpene (Fig. 4A). The COSY spectrum showed couplings between protons H_2-1/H_3-20, H_2-1/H-2, H-2/H_2-3, as well as between H-5/H_2-6, H_2-6/H-7, and H-7/H_3-17 which corroborated rings A and B of the labdane, and confirmed the presence of a hydroxy group at C-2 and a double bond between C-7 and C-8 (Fig. 4A). The remaining NMR signals for the carboxylic acid, a quaternary carbon, three methylene and a methyl group were assigned to the side chain. The COSY crosspeak between H_2-11/H_2-12, and HMBC correlations from H_2-11 to C-9 and C-13, as well as from H_3-16 to C-12, C-13 and C-14 revealed the presence of a pentacyclic ether between C-9 and C-13. Finally, HMBC correlations from H_2-14 to the carbonyl C-15 led to the planar structure of **16**.

The relative configuration was established with the aid of a NOESY spectrum (Fig. 4B), where crosspeaks of H_3-20 with H_3-19 and H_2-11, and of H-5 with H-1a, H-6a, and H_3-18 were indicative of a chair-chair configuration of the decalin substructure [41]. Moreover, a NOESY contact between H_3-20 and H-2 indicated the hydroxyl group to be in α-position. The ether bridge between C-9 and C-13 resulted in a tetrahydrofuran ring with a spiro junction at C-9. The relative configuration at C-13 was established via NOESY crosspeaks observed between H_3-16 and H-1a, and between H-14b and H_3-17.

The ECD spectrum displayed a negative cotton effect at 200 nm (Fig. 4C). In comparison with calculated spectra, the absolute configuration of **16** was determined as (2*S*,5*S*,9*R*,10*S*,13*S*)-2-hydroxygrindelic acid. The best of our knowledge this is the first report of a 2-hydroxygrindelic acid bearing the hydroxy moiety in α-position.

Compound **17** was analyzed by HRESIMS (*m/z* 337.2372 $[M + H]^+$; calcd for $C_{20}H_{33}O_4^+$, 337.2373) and NMR as $C_{20}H_{32}O_4$, a formula requiring five degrees of unsaturation. In the ^1H NMR spectrum resonances for one aldehyde (δ_H 9.47), one olefinic proton (δ_H 6.55), six non-

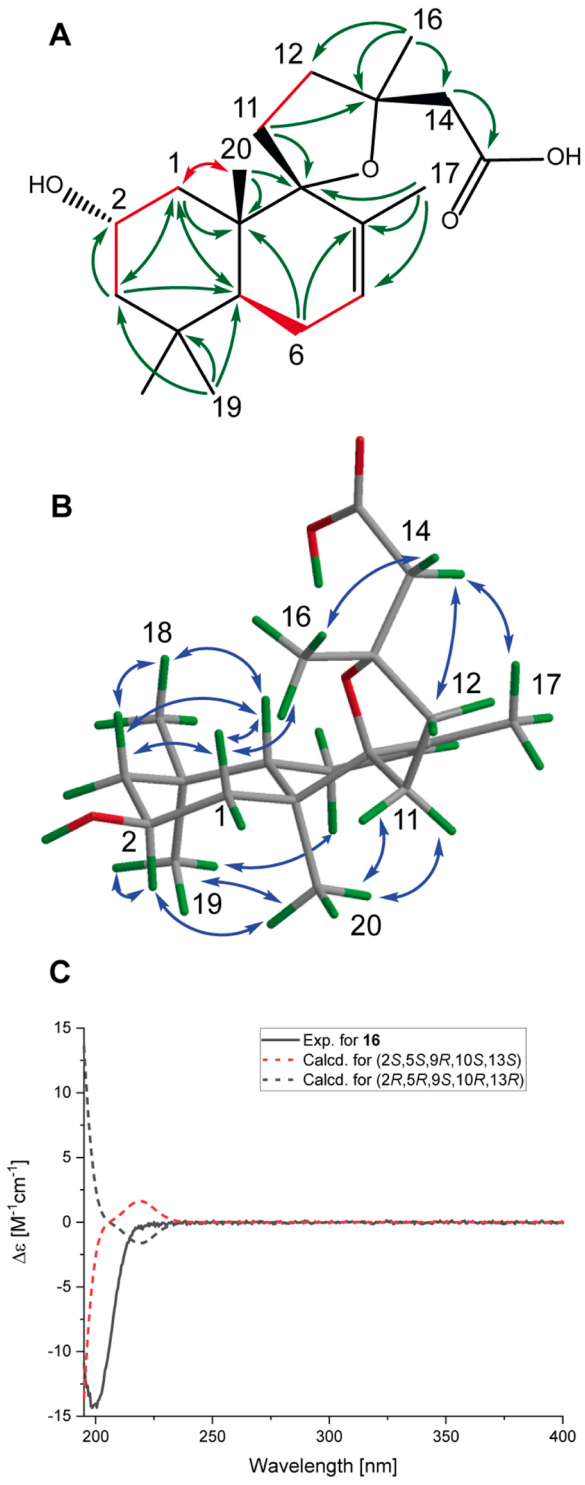

Fig. 4. COSY (red) and key HMBC (green) correlations (A), key NOESY correlations (B), and experimental and calculated ECD spectra (C) of **16.** (For interpretation of the references to colour in this figure legend, the reader is referred to the web version of this article.)

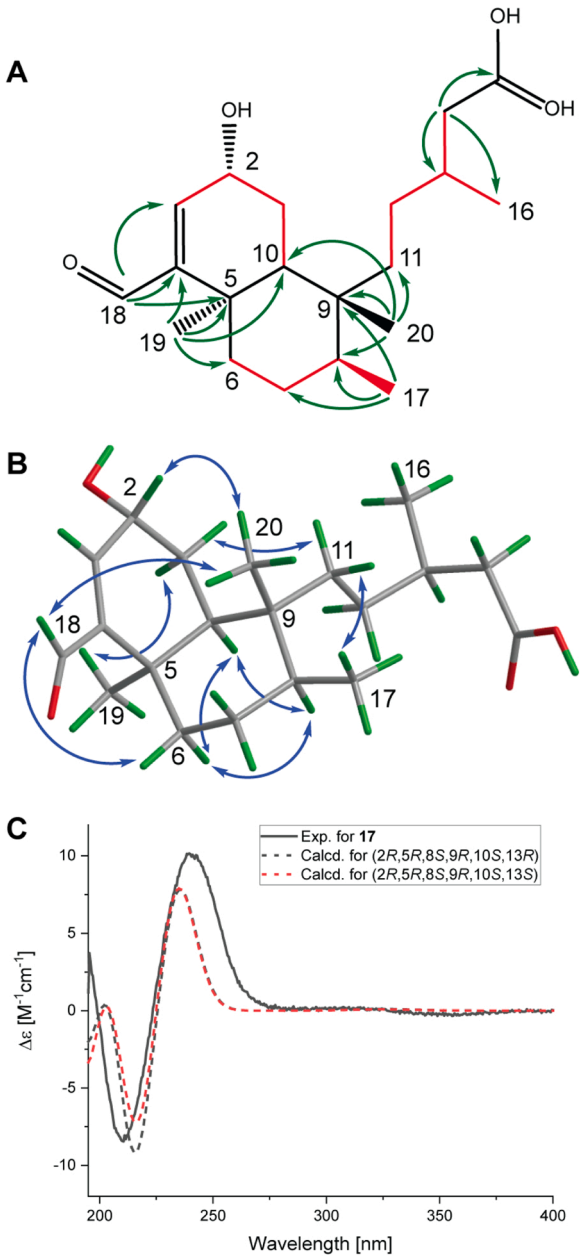

Fig. 5. COSY (red) and key HMBC (green) correlations (A), key NOESY correlations (B), and experimental and calculated ECD spectra (C) of **17.** (For interpretation of the references to colour in this figure legend, the reader is referred to the web version of this article.)

equivalent methylene (δ_H 1.93/2.31, 1.14/3.01, 1.04/1.28, 1.25/1.48, 1.09/1.26, 2.19/2.37), one oxymethine group (δ_H 4.75), three methine (δ_H 1.46, 1.58, 1.91), and four methyl groups (δ_H 0.75, 0.68, 1.01, 1.27), were present. Additionally, in the ^{13}C NMR spectrum the resonance of a carboxylic acid moiety (δ_C 177.7 ppm) was detected. The attachment of the aldehyde at C-4, and methyl groups linked to C-5, C-8 and C-9 were confirmed by key HMBC correlations from H-18 to C-3, C-4, and C-5, from H_3-19 to C-4, C-5, C-6, and C-10, from H_3-17 to C-7, C-8, and C9, and from H_3-20 to C-8, C-9, and C-10. Taken together, these data suggested compound **17** to be a clerodane diterpene (Fig. 5A). In the COSY spectrum a contiguous spin system between H-10 to H-3 was observed, which established the position of the hydroxy group at C-2 and the double bond between C-3 and C-4. A 3-methyl pentanoic acid moiety as the side chain was identified with the aid of HMBC and COSY correlations, and an HMBC cross-peak between H_3-20 and C-11 confirmed the side chain to be attached to C-9.

The relative configuration was established by a NOESY experiment, where crosspeaks between H-8/H-10, and H-10/H_3-19 indicated a *cis*-decalin ring system (Fig. 5B). NOESY contacts between H_3-20/H-2 indicated an α-orientation of the OH-group at C-2. Diterpene **17** was thus a *cis*-clerodane.

The absolute configuration of **17** was determined as

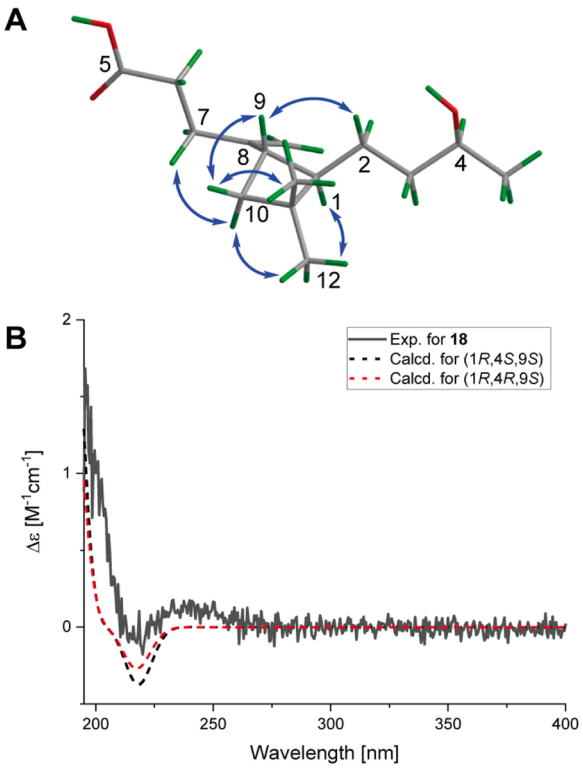

Fig. 6. NOESY correlations (A), experimental and calculated ECD spectra (B, calculated spectrum +15 nm) of compound **18.**

(2*R*,5*R*,8*S*,9*R*,10*S*,13*) by comparison of experimental and calculated ECD spectra (Fig. 5C). Due to the absence of chromophores in the vicinity of C-13, the absolute configuration at this position could not be established. Taken together, **17** was an *ent*-neo-clerodane [42], namely (2*R*,5*R*,8*S*,9*R*,10*S*,13*)-2-hydroxy-clerod-3-en-18-al-15-oic acid. The planar structure of **17** surprisingly appears in a chemical catalogue, even though the compound cannot be found in the literature.

Compound **18** was analyzed by HRESIMS and NMR for $C_{15}H_{26}O_3$, a molecular formula requiring three degrees of unsaturation. In the ^1H NMR spectrum, the presence of two methyl groups (singlets, δ_H 1.05, 1.06), one methylene (δ_H 1.47/1.80) indicative of a cyclobutane, and one exomethylene group (δ_H 4.72 and 4.79) were characteristic for a caryophyllene type sesquiterpene. However, the presence of a carboxyl group (δ_C 178.0) and an unsaturation number of three indicated an opening of the macrocycle. Complete NMR spectral assignments by 1D and 2D NMR data identified **18** as 4-hydroxy-4,5-seco-caryophyllen-5-oic acid, in accord with published data [43]. The relative configuration was determined by a NOESY experiment. Key crosspeaks were observed between H_3-12/H-10a, H-1/H_3-12, H-9/H_2-2, H-9/H-10b, and H-10b/H_3-13 (Fig. 6A). Thus, H-1 and H-9 were on opposite faces of the cyclobutene ring. The absolute configuration of **18** was established as (1*R*,4*,9*S*)-4-hydroxy-4,5-seco-caryophyllen-5-oic acid by comparison of experimental and calculated ECD spectra (Fig. 6B). This was in accord with the absolute configurations of (-)-β-caryophyllene and its derivatives [44]. The absolute configuration at C-4 could not be established due to the lack of a suitable chromophore in the vicinity.

Labdane-type diterpenes and sesquiterpenes have been previously reported in *E. nauseosa* [40], but **17** is the first clerodane diterpene identified in this genus.

3.2. Inhibition of AKT and ERK activity

Compounds **1** - **18** were tested at eight different concentrations (200–1.56 μM) by using the HCS assay enabling the simultaneous readout of ERK and AKT activities [10]. To analyze the activity of structurally diverse flavonoids, the set of isolated compounds was enhanced with the commercially available flavonoid aglycons apigenin, luteolin, kaempferol and quercetin, the methoxylated flavanone hesperetin as well as the flavonoid glycoside isoquercetrin.

Table 1
Activity of selected compounds on the AKT activity in MM121224 cells. IC_{50} values are given with 95% CI.

Compound	IC_{50} values [μM]
3	35.9 ± 6.7
4	54.9 ± 6.5
5	27.0 ± 6.3
6	28.4 ± 3.7
7	21.2 ± 2.7
8	44.7 ± 5.1
9	14.7 ± 1.4
Luteolin	27.9 ± 1.7
Quercetin	41.5 ± 3.5

Compounds were first tested on MM121224 cells. As expected, some compounds clearly inhibited the AKT pathway. Compounds **3–9**, as well as luteolin and quercetin inhibited AKT activity with IC_{50} values < 60 μM (Table 1). Compound **9** was the most active (IC_{50} 14.7 ± 1.4 μM; Fig. 7), while **1**, **10**, **12**, as well as apigenin, kaempferol and hesperetin showed weak inhibition of AKT at 200 μM. The other flavonoids (**2**, **11**, **13-15** and isoquercetrin) as well as terpenes **16-18** were inactive at all test concentrations. In contrast, none of the compounds downregulated ERK activity.

All compounds were also tested in the well-established A2058 human melanoma cell line (Figs. S7-S10, Supporting Information). The activity observed was generally lower in A2058 than in MM121224 cells. Compounds **4–6**, **8** and luteolin showed a marked inhibition at 200 μM, but no IC_{50} values could be determined. Flavonoids **7**, **9** and quercetin weakly inhibited AKT activity at the highest test concentration, whereas the other compounds were inactive (Figs. S7-10, Supporting Information).

To confirm the results obtained with the KTR-based assays, immunostaining experiments were performed in MM121224 cells with anti phospho-ERK and phospho-AKT (serine 473) antibodies. Compounds **4** and **8** were used in this experiment, and measurements of pERK and pAKT (S473) provided similar trends than the ERK/AKT-KTR readouts. pAKT was lowered in a concentration-dependent manner, and pERK was slightly increased (Fig. S11, Supporting Information). This striking behavior of AKT inhibition and slight ERK activation could emerge, because AKT inhibition might affect a crosstalk with ERK, or because **4** and **8** affect other kinases, which in turn could lead to a slight ERK activation via negative regulation of phosphatases [45].

With a set of structurally diverse flavonoids at hand, some preliminary structure-activity information could be derived from the data. First, flavones were more active than flavanones. Furthermore, flavones with two substituents on the ring B seemed to be more potent inhibitors of the AKT activity than flavones with one or no substituents. Interestingly, the flavonol glycoside isoquercetin was inactive, as compared to the active aglycone quercetine. However, additional flavonoids glycosides should be tested to corroborate this observation.

Given that the assay readout is measuring the activity downstream of the signaling cascades, the specific targets of the flavonoids remain to be identified. Also, the compounds might target several proteins in the network, and may show differing patterns of inhibition on these proteins.

3.3. Physicochemical and ADME properties

Physiochemical and ADME properties as defined by Lipinski and Veber rules [46,47], were calculated for all compounds, as a preliminary assessment of their drug-likeness (Table S7). Values for compounds **1-18** were all in accordance with Lipinski's rule of five, with clog P values

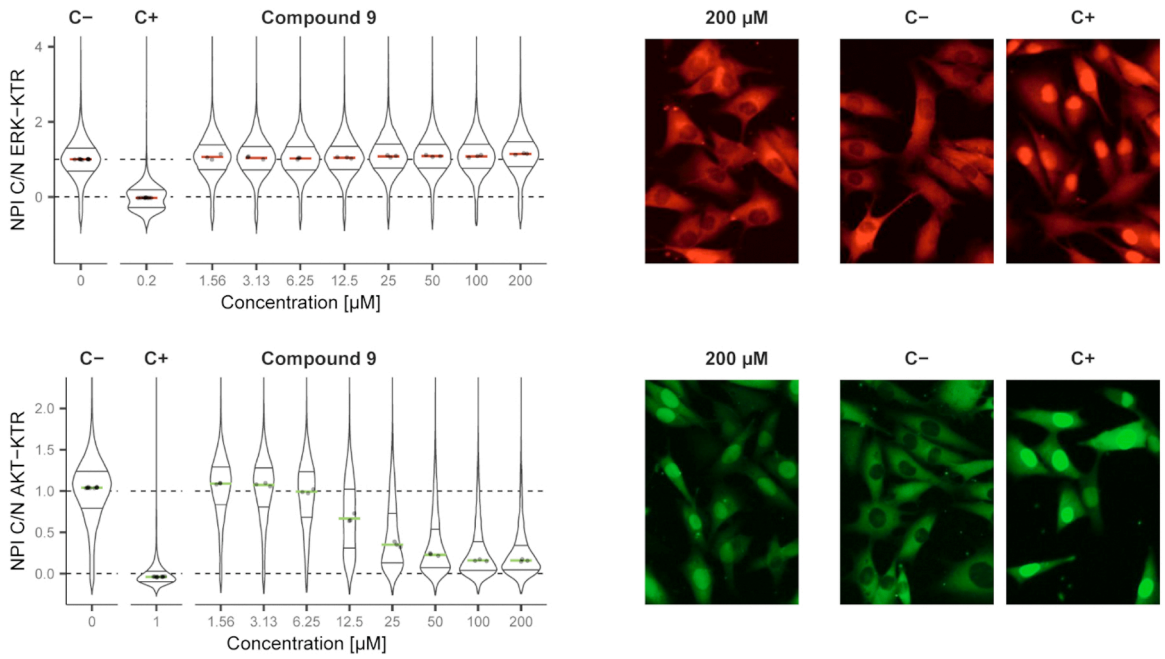

Fig. 7. Concentration-response curves for compound **9** in MM121224 cells. ERK (top) and AKT (bottom) activity is shown, together with representative images (right). C+ and C- designate positive (1 μM GDC0941 as PI3K/AKT pathway inhibitor, 200 nM cobimetinib as MAPK/ERK pathway inhibitor) and negative (0.75% DMSO) controls, respectively. Data distribution recorded in single MM121224 cells are represented as violin plots, and median of treatment distribution (middle bar), as well as first and third quartiles are shown. Data are taken from at least 200 cells.

between 0.87 and 4.21, a molecular weight ranging from 254 to 330 g/mol, with two to four H donor and three to eight H acceptor sites, one to eight rotatable bonds, and one to three rings. Predicted solubility ranged from 0.33 mg/mL (soluble) to 0.03 mg/mL (highly insoluble), and Caco-2 permeability from 111×10^6 cm/s (highly permeable) to 4.6×10^6 cm/s (moderately permeable). The predicted plasma protein binding (PPB) of compounds was moderate to extensive (70–96%). Compounds **15** and **17** were predicted to be permeable into the CNS, whereas the others were either weekly or non-penetrating. Human intestinal absorption (HIA) for all compounds was predicted as 100%.

Taken together, the isoprenoids had the best overall ADME properties when considering solubility, permeability and plasma protein binding. The most active flavonoid **9** showed high predicted permeability in Caco-2 and intestinal absorption, but had a very low calculated solubility, extensive plasma protein binding, and no CNS penetration.

4. Conclusion

The HPLC-based activity profiling approach was used to localize compounds present in the active time window of the DCM extract of *Ericameria nauseosa*. The activity profile guided the scale-up isolation and afforded 18 compounds with different natural product scaffolds, including 11 flavones (**1-11**), four flavanones (**12-15**), a labdane diterpene (**16**), a clerodane diterpene (**17**), and a seco-caryophyllene (**18**). Flavonoids were found to be responsible for the inhibition of AKT activity of the extract, while none of the terpenes was active. Nevertheless, to our knowledge the two diterpenes are new natural products and were identified as (2*S*,5*S*,9*R*,10*S*,13*S*)-2-hydroxygrindelic acid (**16**) and (2*R*,5*R*,8*S*,9*R*,10*S*,13*)-2-hydroxy-clerod-3-en-18-al-15-oic acid (**17**). Interestingly, **17** constitutes the first report of a clerodane type diterpene in the genus *Ericameria*. We also established the absolute configuration of (1*R*,4*,9*S*)-4-hydroxy-4,5-seco-caryophyllen-5-oic acid (**18**) and found it to be consistent with its likely biosynthetic precursor (-)-β-caryophyllene [44].

The methoxylated flavone **9** was the most potent compound, with an IC_{50} value of 14.7 ± 1.4 μM. This is the first report of the activity of **9** as an inhibitor of the PI3K/AKT pathway. Additional experiments are now planned to determine the target protein(s) for that compound. Other methoxylated flavonoids **3-8,** as well as quercetin and luteolin were also considered as active on the AKT pathway (IC_{50} values between 20 and 55 μM). Similar results were obtained in a recent metabolomic study [48]. The diverse set of flavonoids isolated in the present investigation enabled a preliminary analysis of structure-activity relationship. Flavones were shown to be more active than flavanones. In addition, the presence of two substituents on the ring B seemed to have a positive effect on the potency.

Activity of flavonoids on the PI3K/AKT pathway has been already reported [49–55], such as for quercetin and luteolin tested in our study [49–54]. Interestingly, in a docking study, luteolin was shown to interact with PI3K in a binding pose similar to that of the ATP-competitive inhibitor LY294002 [55], a synthetic flavonoid analog [56]. Moreover, the flavonoid alkaloid analog alvocidib is an inhibitor of cycline dependent kinases that has been shown to have promising anti-cancer activity [57–59]. A prodrug of alvocidib is currently in clinical trial for the treatment advanced solid tumors. These examples illustrate the potential of flavonoids as promising scaffolds for the development of new anticancer drugs [60,61].

CRediT authorship contribution statement

TH performed extraction, isolation, structure elucidation, biological experiments and *in silico* calculations. MD developed the image and data analysis pipeline in R. FG assisted in isolation, and JKR assisted in the analysis of NMR and ECD spectra and revised the respective parts of the manuscript. LD was involved in preliminary data acquisition. EG supervised the project with the support of MH. MH collected the plant material. TH wrote the draft manuscript which was finalized by OP, MH and EG. All authors read and approved the final manuscript.

Conflict of interest statement

The authors declare that they have no known competing financial interests or personal relationships that could have appeared to influence the work reported in this paper.

Acknowledgements

We thank Mitchell Levesque (University Hospital of Zurich) for providing MM121224 patient-derived cells, and Matthias Wymann (Department of Biomedicine, University of Basel) for A2058 cells. We thank Alberto Mattei for transfecting cells with the biosensors for ERK, AKT-KTR, and H2B. We are grateful to the DBM Microscopy Core Facility (Department of Biomedicine, University of Basel), especially Pascal Lorentz, for access to the HCS microscope and for technical support. ECD spectra were measured at the Biophysics Facility, Biozentrum, University of Basel. This work was supported by a grant of the Swiss National Science Foundation (205321–176008, to Matthias Hamburger and Olivier Pertz) and the Swiss Cancer League (KFS-3727–08-2015 to Olivier Pertz).

Appendix A. Supporting information

Supplementary data associated with this article can be found in the online version at doi:10.1016/j.biopha.2022.113754.

References

[1] N.H. Matthews, W.-Q. Li, A.A. Qureshi, M.A. Weinstock, E. Cho, Epidemiology of Melanoma, in: W.H. Ward, J.M. Farma (Eds.), Cutan. Melanoma Etiol. Ther., Codon Publications, Brisbane, 2017, pp. 3–22.

[2] A. De Luca, M.R. Maiello, A. D'Alessio, M. Pergameno, N. Normanno, The RAS/RAF/MEK/ERK and the PI3K/AKT signalling pathways: role in cancer pathogenesis and implications for therapeutic approaches, Expert Opin. Ther. Targets 16 (2012) S17–S27, https://doi.org/10.1517/14728222.2011.639361.

[3] H. Davies, G.R. Bignell, C. Cox, P. Stephens, S. Edkins, S. Clegg, J. Teague, H. Woffendin, M.J. Garnett, W. Bottomley, N. Davis, E. Dicks, R. Ewing, Y. Floyd, K. Gray, S. Hall, R. Hawes, J. Hughes, V. Kosmidou, A. Menzies, C. Mould, A. Parker, C. Stevens, S. Watt, S. Hooper, R. Wilson, H. Jayatilake, B.A. Gusterson, C. Cooper, J. Shipley, D. Hargrave, K. Pritchard-Jones, N. Maitland, G. Chenevix-Trench, G.J. Riggins, D.D. Bigner, G. Palmieri, A. Cossu, A. Flanagan, A. Nicholson, J.W.C. Ho, S.Y. Leung, S.T. Yuen, B.L. Weber, H.F. Seigler, T.L. Darrow, H. Paterson, R. Marais, C.J. Marshall, R. Wooster, M.R. Stratton, P.A. Futreal, Mutations of the BRAF gene in human cancer, Nature 417 (2002) 949–954, https://doi.org/10.1038/nature00766.

[4] R. Akbani, K.C. Akdemir, B.A. Aksoy, M. Albert, A. Ally, S.B. Amin, H. Arachchi, A. Arora, J.T. Auman, B. Ayala, J. Baboud, M. Balasundaram, S. Balu, N. Barnabas, J. Bartlett, P. Bartlett, B.C. Bastian, S.B. Baylin, M. Behera, D. Belyaev, C. Benz, B. Bernard, R. Beroukhim, N. Bir, A.D. Black, T. Bodenheimer, L. Boice, G. M. Boland, R. Bono, M.S. Bootwalla, M. Bosenberg, J. Bowen, R. Bowlby, C. A. Bristow, L. Brockway-Lunardi, D. Brooks, J. Brzezinski, W. Bshara, E. Buda, W. R. Burns, Y.S.N. Butterfield, M. Button, T. Calderone, G.A. Cappellini, C. Carter, S. L. Carter, L. Cherney, A.D. Cherniack, A. Chevalier, L. Chin, J. Cho, R.J. Cho, Y.-L. Choi, A. Chu, S. Chudamani, K. Cibulskis, G. Ciriello, A. Clarke, S. Coons, L. Cope, D. Crain, E. Curley, L. Danilova, S. D'Atri, T. Davidsen, M.A. Davies, K. A. Delman, J.A. Demchok, Q.A. Deng, Y.L. Deribe, N. Dhalla, R. Dhir, D. DiCara, M. Dinikin, M. Dubina, J.S. Ebrom, S. Egea, G. Eley, J. Engel, J.M. Eschbacher, K. V. Fedosenko, I. Felau, T. Fennell, M.L. Ferguson, S. Fisher, K.T. Flaherty, S. Frazer, J. Frick, V. Fulidou, S.B. Gabriel, J. Gao, J. Gardner, L.A. Garraway, J.M. Gastier-Foster, C. Gaudioso, N. Gehlenborg, G. Genovese, M. Gerken, J.E. Gershenwald, G. Getz, C. Gomez-Fernandez, T. Gribbin, J. Grimsby, B. Gross, R. Guin, T. Gutschner, A. Hadjipanayis, R. Halaban, B. Hanf, D. Haussler, L.E. Haydu, D. N. Hayes, N.K. Hayward, D.I. Heiman, L. Herbert, J.G. Herman, P. Hersey, K. A. Hoadley, E. Hodis, R.A. Holt, D.S.B. Hoon, S. Hoppough, A.P. Hoyle, F. W. Huang, M. Huang, S. Huang, C.M. Hutter, M. Ibbs, L. Iype, A. Jacobsen, V. Jakrot, A. Janning, W.R. Jeck, S.R. Jefferys, M.A. Jensen, C.D. Jones, S.J. M. Jones, Z. Ju, H. Kakavand, H. Kang, R.F. Kefford, F.R. Khuri, J. Kim, J. M. Kirkwood, J. Klode, A. Korkut, K. Korski, M. Krauthammer, R. Kucherlapati, L. N. Kwong, W. Kycler, M. Ladanyi, P.H. Lai, P.W. Laird, E. Lander, M.S. Lawrence, A.J. Lazar, R. Łaźniak, D. Lee, J.E. Lee, J. Lee, K. Lee, S. Lee, W. Lee, E. Leporowska, K.M. Leraas, H.I. Li, T.M. Lichtenberg, L. Lichtenstein, P. Lin, S. Ling, J. Liu, O. Liu, W. Liu, G.V. Long, Y. Lu, S. Ma, Y. Ma, A. Mackiewicz, H. S. Mahadeshwar, J. Malke, D. Mallery, G.M. Manikhas, G.J. Mann, M.A. Marra, B. Matejka, M. Mayo, S. Mehrabi, S. Meng, M. Meyerson, P.A. Mieczkowski, J. P. Miller, M.L. Miller, G.B. Mills, F. Moiseenko, R.A. Moore, S. Morris, C. Morrison, D. Morton, S. Moschos, L.E. Mose, F.L. Muller, A.J. Mungall, D. Murawa, P. Murawa, B.A. Murray, L. Nezi, S. Ng, D. Nicholson, M.S. Noble, A. Osunkoya, T. K. Owonikoko, B.A. Ozenberger, E. Pagani, O.V. Paklina, A. Pantazi, M. Parfenov, J. Parfitt, P.J. Park, W.-Y. Park, J.S. Parker, F. Passarelli, R. Penny, C.M. Perou, T. D. Pihl, O. Potapova, V.G. Prieto, A. Protopopov, M.J. Quinn, A. Radenbaugh, K. Rai, S.S. Ramalingam, A.T. Raman, N.C. Ramirez, R. Ramirez, U. Rao, W. K. Rathmell, X. Ren, S.M. Reynolds, J. Roach, A.G. Robertson, M.I. Ross, J. Roszik, G. Russo, G. Saksena, C. Saller, Y. Samuels, C. Sander, C. Sander, G. Sandusky, N. Santoso, M. Saul, R.P.M. Saw, D. Schadendorf, J.E. Schein, N. Schultz, S. E. Schumacher, C. Schwallier, R.A. Scolyer, J. Seidman, P.C. Sekhar, H.S. Sekhon, Y. Senbabaoglu, S. Seth, K.F. Shannon, S. Sharpe, N.E. Sharpless, K.R.M. Shaw, C. Shelton, T. Shelton, R. Shen, M. Sheth, Y. Shi, C.J. Shiau, I. Shmulevich, G. L. Sica, J.V. Simons, R. Sinha, P. Sipahimalani, H.J. Sofia, M.G. Soloway, X. Song, C. Sougnez, A.J. Spillane, A. Spychała, J.R. Stretch, J. Stuart, W.M. Suchorska, A. Sucker, S.O. Sumer, Y. Sun, M. Synott, B. Tabak, T.R. Tabler, A. Tam, D. Tan, J. Tang, R. Tarnuzzer, K. Tarvin, H. Tatka, B.S. Taylor, M. Teresiak, N. Thiessen, J. F. Thompson, L. Thorne, V. Thorsson, J.M. Trent, T.J. Triche, K.Y. Tsai, P. Tsou, D. J. Van Den Berg, E.M. Van Allen, U. Veluvolu, R.G. Verhaak, D. Voet, O. Voronina, V. Walter, J.S. Walton, Y. Wan, Y. Wang, Z. Wang, S. Waring, I.R. Watson, N. Weinhold, J.N. Weinstein, D.J. Weisenberger, P. White, M.D. Wilkerson, J. S. Wilmott, L. Wise, M. Wiznerowicz, S.E. Woodman, C.-J. Wu, C.-C. Wu, J. Wu, Y. Wu, R. Xi, A.W. Xu, D. Yang, L. Yang, L. Yang, T.I. Zack, J.C. Zenklusen, H. Zhang, J. Zhang, W. Zhang, X. Zhao, J. Zhu, K. Zhu, L. Zimmer, E. Zmuda, L. Zou, Genomic classification of cutaneous melanoma, Cell 161 (2015) 1681–1696, https://doi.org/10.1016/j.cell.2015.05.044.

[5] E.J. Davis, D.B. Johnson, J.A. Sosman, S. Chandra, Melanoma: what do all the mutations mean? Cancer 124 (2018) 3490–3499, https://doi.org/10.1002/cncr.31345.

[6] J.A. Sosman, K.B. Kim, L. Schuchter, R. Gonzalez, A.C. Pavlick, J.S. Weber, G. A. McArthur, T.E. Hutson, S.J. Moschos, K.T. Flaherty, P. Hersey, R. Kefford, D. Lawrence, I. Puzanov, K.D. Lewis, R.K. Amaravadi, B. Chmielowski, H. J. Lawrence, Y. Shyr, F. Ye, J. Li, K.B. Nolop, R.J. Lee, A.K. Joe, A. Ribas, Survival in BRAF V600–mutant advanced melanoma treated with vemurafenib, N. Engl. J. Med. 366 (2012) 707–714, https://doi.org/10.1056/NEJMoa1112302.

[7] A. Hauschild, J.-J. Grob, L.V. Demidov, T. Jouary, R. Gutzmer, M. Millward, P. Rutkowski, C.U. Blank, W.H. Miller, E. Kaempgen, S. Martín-Algarra, B. Karaszewska, C. Mauch, V. Chiarion-Sileni, A.-M. Martin, S. Swann, P. Haney, B. Mirakhur, M.E. Guckert, V. Goodman, P.B. Chapman, Dabrafenib in BRAF-mutated metastatic melanoma: a multicentre, open-label, phase 3 randomised controlled trial, Lancet 380 (2012) 358–365, https://doi.org/10.1016/S0140-6736(12)60868-X.

[8] E.T. Tanda, I. Vanni, A. Boutros, V. Andreotti, W. Bruno, P. Ghiorzo, F. Spagnolo, Current state of target treatment in BRAF mutated melanoma, Front. Mol. Biosci. 7 (2020) 154, https://doi.org/10.3389/fmolb.2020.00154.

[9] Melanoma of the Skin - Cancer Stat Facts, National Cancer Institute - SEER, Natl. Cancer Inst. - SEER. (2020). ⟨https://seer.cancer.gov/statfacts/html/melan.html⟩ (accessed January 28, 2022).

[10] L. Dürr, T. Hell, M. Dobrzyński, A. Mattei, A. John, N. Augsburger, G. Bradanini, J. K. Reinhardt, F. Rossberg, M. Drobnjakovic, M.P. Gupta, M. Hamburger, O. Pertz, E. Garo, High-content screening pipeline for natural products targeting oncogenic signaling in melanoma, J. Nat. Prod. (2022), https://doi.org/10.1021/acs.jnatprod.1c01154.

[11] M.I.G. Raaijmakers, D.S. Widmer, A. Narechania, O. Eichhoff, S.N. Freiberger, J. Wenzina, P.F. Cheng, D. Mihic-Probst, R. Desalle, R. Dummer, M.P. Levesque, Co-existence of BRAF and NRAS driver mutations in the same melanoma cells results in heterogeneity of targeted therapy resistance, Oncotarget 7 (2016) 77163–77174, https://doi.org/10.18632/oncotarget.12848.

[12] S. Regot, J.J. Hughey, B.T. Bajar, S. Carrasco, M.W. Covert, High-sensitivity measurements of multiple kinase activities in live single cells, Cell 157 (2014) 1724–1734, https://doi.org/10.1016/j.cell.2014.04.039.

[13] R.P. Roberts, L.E. Urbatsch, Molecular phylogeny of *Chrysothamnus* and related genera (Asteraceae, Astereae) based on nuclear ribosomal 3′ ETS and ITS sequence data, Syst. Bot. 29 (2004) 199–215, https://doi.org/10.1600/036364404772973410.

[14] G.L. Nesom, G.I. Baird, Completion of *Ericameria* (Asteraceae: Astereae), diminution of *Chrysothamnus*, Phytologia 75 (1993) 74–93.

[15] P.L. Scheinost, J. Scianna, P.L. Ogle. Plant guide for rubber rabbitbrush (*Ericameria nauseosa*), USDA-Natural Resources Conservation Service, Pullman Plant Materials, Center, Pullman, WA, 2010.

[16] A.F. Rose, Grindelane diterpenoids from *Chrysothamnus nauseosus*, Phytochemistry 19 (1980) 2689–2693, https://doi.org/10.1016/S0031-9422(00)83945-X.

[17] J.F. Stevens, E. Wollenweber, M. Ivancic, V.L. Hsu, S. Sundberg, M.L. Deinzer, Leaf surface flavonoids of *Chrysothamnus*, Phytochemistry 51 (1999) 771–780, https://doi.org/10.1016/S0031-9422(99)00110-7.

[18] S. Chao, D.G. Young, H. Casabianca, M.-C. Bertrand, Composition of the oils of three *Chrysothamnus nauseosus* varieties, J. Essent. Oil Res. 15 (2003) 425–427, https://doi.org/10.1080/10412905.2003.9698630.

[19] A.F. Rose, B.A. Butt, T. Jermy, Polyacetylenes from the rabbitbrush, *Chrysothamnus nauseosus*, Phytochemistry 19 (1980) 563–566, https://doi.org/10.1016/0031-9422(80)87015-4.

[20] O. Potterat, M. Hamburger, Combined use of extract libraries and HPLC-based activity profiling for lead discovery: potential, challenges, and practical considerations, Planta Med. 80 (2014) 1171–1181, https://doi.org/10.1055/s-0034-1382900.

[21] M.J. Frisch, G.W. Trucks, H.B. Schlegel, G.E. Scuseria, M.A. Robb, J.R. Cheeseman, G. Scalmani, V. Barone, G.A. Petersson, H. Nakatsuji, X. Li, M. Caricato, A. Marenich, J. Bloino, B.G. Janesko, R. Gomperts, B. Mennucci, H.P. Hratchian, J.V. Ortiz, A.F. Izmaylov, J.L. Sonnenberg, D. Williams-Young, F. Ding, F. Lipparini, F. Egidi, J. Goings, B. Peng, A. Petrone, T. Henderson, D. Ranasinghe, V.G. Zakrzewski, J. Gao, N. Rega, G. Zheng, W. Liang, M. Hada, M. Ehara, K. Toyota, R. Fukuda, J. Hasegawa, M. Ishida, T. Nakajima, Y. Honda, O. Kitao, H. Naka, T. Vreven, K. Throssell, J.A. Montgomery, J.E. Peralta, F. Ogliaro, M. Bearpark, J.J. Heyd, E. Brothers, K.N. Kudin, V.N. Staroverov, T. Keith, R. Kobayashi, J. Normand, K. Raghavachari, A. Rendel, J.C. Burant, S.S. Iyengar, J. Tomasi, M. Cossi, J.M. Millam, M. Klene, C. Adamo, R. Cammi, J.W. Ochterski, R.L. Martin, K. Morokuma, O. Farkas, J.B. Foresman, D.J. Fox, Gaussian 09, Revision D.01,

Gaussian 09, Revision D.01. (n.d.). https://gaussian.com/g09citation/ (accessed February 9, 2022).
[22] T. Bruhn, A. Schaumlöffel, Y. Hemberger, G. Bringmann, SpecDis: quantifying the comparison of calculated and experimental electronic circular dichroism spectra: UV AND ECD EVALUATION WITH SPECDIS, Chirality 25 (2013) 243–249, https://doi.org/10.1002/chir.22138.
[23] J.B. Harborne, T.J. Mabry, H. Mabry (Eds.), The Flavonoids, Chapman & Hall, London, 1975.
[24] T. Horie, M. Tsukayama, Y. Kawamura, M. Seno, Studies of the selective O-alkylation and dealkylation of flavonoids. 10. Selective demethylation of 7-hydroxy-3,5,8-trimethoxyflavones with anhydrous aluminum halide in acetonitrile or ether, J. Org. Chem. 52 (1987) 4702–4709, https://doi.org/10.1021/jo00230a009.
[25] M. Higa, M. Imamura, K. Ogihara, T. Suzuka, Isolation of five new flavonoids from *Melicope triphylla*, Chem. Pharm. Bull. (Tokyo). 61 (2013) 384–389, https://doi.org/10.1248/cpb.c12-00940.
[26] K. Fukui, T. Matsumoto, S. Tanaka, Synthetic studies of the flavone derivatives. XI. The synthesis of 4′,5,7-trihydroxy-3,8-dimethoxyflavone, a pigment from *Cyanostegia angustifolia* Turcz, Bull. Chem. Soc. Jpn 42 (1969) 2380–2382, https://doi.org/10.1246/bcsj.42.2380.
[27] M.L. Docampo-Palacios, A. Alvarez-Hernández, O. Adiji, D. Gamiotea-Turro, A. B. Valerino-Diaz, L.P. Viegas, I.E. Ndukwe, Â. de Fátima, C. Heiss, P. Azadi, G. M. Pasinetti, R.A. Dixon, Glucuronidation of methylated quercetin derivatives: chemical and biochemical approaches, J. Agric. Food Chem. 68 (2020) 14790–14807, https://doi.org/10.1021/acs.jafc.0c04500.
[28] A. Arciniegas, L.A. Polindara, A.L. Pérez-Castorena, A.M. García, G. Avila, J. L. Villaseñor, A.R. de Vivar, Chemical composition and biological activity of *Laennecia schiedeana*, Z. Für Naturforsch. C. 66 (2011) 115–122, https://doi.org/10.1515/znc-2011-3-404.
[29] T. Horie, The syntheses of centaureidin and 5,7,3′-trihydroxy-3,8,4′-trimethoxyflavone, Experientia 24 (1968) 880–881, https://doi.org/10.1007/BF02138625.
[30] Y. Wang, M. Hamburger, J. Gueho, K. Hostettmann, Antimicrobial flavonoids from *Psiadia trinervia* and their methylated and acetylated derivatives, Phytochemistry 28 (1989) 2323–2327, https://doi.org/10.1016/S0031-9422(00)97976-7.
[31] S.E. Bianchi, S. Kaiser, V. Pittol, E. Doneda, K.C.B. De Souza, V.L. Bassani, Semi-preparative isolation and purification of phenolic compounds from *Achyrocline satureioides* (Lam) D.C. by high-performance counter-current chromatography, Phytochem. Anal. 30 (2019) 182–192, https://doi.org/10.1002/pca.2803.
[32] M. Hosny, K. Dhar, J.P.N. Rosazza, Hydroxylations and Methylations of Quercetin, Fisetin, and Catechin by *Streptomyces griseus*, J. Nat. Prod. 64 (2001) 462–465, https://doi.org/10.1021/np000457m.
[33] L. Yang, J. Lin, B. Zhou, Y. Liu, B. Zhu, Activity of compounds from *Taxillus sutchuenensis* as inhibitors of HCV NS3 serine protease, Nat. Prod. Res. 31 (2017) 487–491, https://doi.org/10.1080/14786419.2016.1190719.
[34] S. Amador, A. Nieto-Camacho, Ma.T. Ramírez-Apan, M. Martínez, E. Maldonado, Cytotoxic, anti-inflammatory, and α-glucosidase inhibitory effects of flavonoids from *Lippia graveolens* (Mexican oregano), Med. Chem. Res. 29 (2020) 1497–1506, https://doi.org/10.1007/s00044-020-02569-6.
[35] A. Bouaroura, N. Segueni, JesusG. Diaz, C. Bensouici, S. Akkal, S. Rhouati, Preliminary analysis of the chemical composition, antioxidant and anticholinesterase activities of Algerian propolis, Nat. Prod. Res. 34 (2020) 3257–3261, https://doi.org/10.1080/14786419.2018.1556658.
[36] S. Jew, H. Kim, S. Bae, J. Kim, H. Park*, Enantioselective synthetic method for 3-hydroxyflavanones: an approach to (2R,3R)-3′,4′-O-dimethyltaxifolin, Tetrahedron Lett. 41 (2000) 7925–7928, https://doi.org/10.1016/S0040-4039(00)01382-4.
[37] C. Hu, Z. Zhou, Y. Xiang, X. Song, H. Wang, K. Tao, X. Ye, Design, synthesis and anti-inflammatory activity of dihydroflavonol derivatives, Med. Chem. Res. 27 (2018) 194–205, https://doi.org/10.1007/s00044-017-2054-z.
[38] Y.-L. Huang, C.-C. Chen, F.-L. Hsu, C.-F. Chen, Two tannins from *Phyllanthus tenellus*, J. Nat. Prod. 61 (1998) 523–524, https://doi.org/10.1021/np970428k.
[39] F. Hanawa, T. Yamada, T. Nakashima, Phytoalexins from *Pinus strobus* bark infected with pinewood nematode, *Bursaphelenchus xylophilus*, Phytochemistry 57 (2001) 223–228, https://doi.org/10.1016/S0031-9422(00)00514-8.
[40] F. Bohlmann, D. Lakshmi, H. Robinson, R.M. King, Neue Labdan-Derivate aus *Chrysothamnus nauseosus*, Phytochemistry 19 (1979) 1889–1892.
[41] R.J. Peters, Two rings in them all: The labdane -related diterpenoids, Nat. Prod. Rep. 27 (2010) 1521–1530, https://doi.org/10.1039/C0NP00019A.
[42] R. Li, S.L. Morris-Natschke, K.-H. Lee, Clerodane diterpenes: sources, structures, and biological activities, Nat. Prod. Rep. 33 (2016) 1166–1226, https://doi.org/10.1039/C5NP00137D.
[43] L. Quijano, A. Vasquez-C, T. Ríos, Sesquiterpene lactones and a seco-caryophyllene derivative from *Montanoa karwinskii*, Phytochemistry 38 (1995) 1251–1255, https://doi.org/10.1016/0031-9422(94)00791-Q.
[44] L.-M. Deng, L.-J. Hu, W. Tang, J.-X. Liu, X.-J. Huang, Y.-Y. Li, Y.-L. Li, W.-C. Ye, Y. Wang, A biomimetic synthesis-enabled stereochemical assignment of rhodotomentones A and B, two unusual caryophyllene-derived meroterpenoids from *Rhodomyrtus tomentosa*, Org. Chem. Front. 8 (2021) 5728–5735, https://doi.org/10.1039/D1QO00989C.
[45] M.C. Mendoza, E.E. Er, J. Blenis, The Ras-ERK and PI3K-mTOR pathways: cross-talk and compensation, Trends Biochem. Sci. 36 (2011) 320–328, https://doi.org/10.1016/j.tibs.2011.03.006.
[46] C.A. Lipinski, F. Lombardo, B.W. Dominy, P.J. Feeney, Experimental and computational approaches to estimate solubility and permeability in drug discovery and development settings, Adv. Drug Deliv. Rev. 23 (1997) 3–25, https://doi.org/10.1016/S0169-409X(96)00423-1.
[47] D.F. Veber, S.R. Johnson, H.-Y. Cheng, B.R. Smith, K.W. Ward, K.D. Kopple, Molecular properties that influence the oral bioavailability of drug candidates, J. Med. Chem. 45 (2002) 2615–2623, https://doi.org/10.1021/jm020017n.
[48] T. Hell, A. Rutz, L. Dürr, M. Dobrzyński, J.K. Reinhardt, T. Lehner, M. Keller, A. John, M. Gupta, O. Pertz, M. Hamburger, J.-L. Wolfender, E. Garo, Combining activity profiling with advanced annotation to accelerate the discovery of natural products targeting oncogenic signaling in melanoma, J. Nat. Prod. (2022), https://doi.org/10.1021/acs.jnatprod.2c00146.
[49] J. Zhao, L. Li, Z. Wang, L. Li, M. He, S. Han, Y. Dong, X. Liu, W. Zhao, Y. Ke, C. Wang, Luteolin attenuates cancer cell stemness in PTX-resistant oesophageal cancer cells through mediating SOX2 protein stability, Pharmacol. Res. 174 (2021), 105939, https://doi.org/10.1016/j.phrs.2021.105939.
[50] M.-L. Shi, Y.-F. Chen, W.-Q. Wu, Y. Lai, Q. Jin, W.-L. Qiu, D.-L. Yu, Y.-Z. Li, H.-F. Liao, Luteolin inhibits the proliferation, adhesion, migration and invasion of choroidal melanoma cells in vitro, Exp. Eye Res. 210 (2021), 108643, https://doi.org/10.1016/j.exer.2021.108643.
[51] M.T. Cook, Mechanism of metastasis suppression by luteolin in breast cancer, Breast Cancer Targets Ther. 10 (2018) 89–100, https://doi.org/10.2147/BCTT.S144202.
[52] C.-H. Lin, C.-Y. Chang, K.-R. Lee, H.-J. Lin, T.-H. Chen, L. Wan, Flavones inhibit breast cancer proliferation through the Akt/FOXO3a signaling pathway, BMC Cancer 15 (2015) 958, https://doi.org/10.1186/s12885-015-1965-7.
[53] A.B. Ward, H. Mir, N. Kapur, D.N. Gales, P.P. Carriere, S. Singh, Quercetin inhibits prostate cancer by attenuating cell survival and inhibiting anti-apoptotic pathways, World J. Surg. Oncol. 16 (2018) 108, https://doi.org/10.1186/s12957-018-1400-z.
[54] Y. Ji, L. Li, Y.-X. Ma, W.-T. Li, L. Li, H.-Z. Zhu, M.-H. Wu, J.-R. Zhou, Quercetin inhibits growth of hepatocellular carcinoma by apoptosis induction in part via autophagy stimulation in mice, J. Nutr. Biochem 69 (2019) 108–119, https://doi.org/10.1016/j.jnutbio.2019.03.018.
[55] A. Sain, T. Kandasamy, D. Naskar, In silico approach to target PI3K/Akt/mTOR axis by selected *Olea europaea* phenols in PIK3CA mutant colorectal cancer, J. Biomol. Struct. Dyn. 0 (2021) 1–16, https://doi.org/10.1080/07391102.2021.1953603.
[56] Y. Imai, H. Yamagishi, Y. Ono, Y. Ueda, Versatile inhibitory effects of the flavonoid-derived PI3K/Akt inhibitor, LY294002, on ATP-binding cassette transporters that characterize stem cells, Clin. Transl. Med. 1 (2012), e24, https://doi.org/10.1186/2001-1326-1-24.
[57] L.R. Kelland, Flavopiridol, the first cyclin-dependent kinase inhibitor to enter the clinic: current status, Expert Opin. Investig. Drugs 9 (2000) 2903–2911, https://doi.org/10.1517/13543784.9.12.2903.
[58] J.F. Zeidner, J.E. Karp, Clinical activity of alvocidib (flavopiridol) in acute myeloid leukemia, Leuk. Res. 39 (2015) 1312–1318, https://doi.org/10.1016/j.leukres.2015.10.010.
[59] J.F. Zeidner, M.C. Foster, A.L. Blackford, M.R. Litzow, L.E. Morris, S.A. Strickland, J.E. Lancet, P. Bose, M.Y. Levy, R. Tibes, I. Gojo, C.D. Gocke, G.L. Rosner, R. F. Little, J.J. Wright, L.A. Doyle, B.D. Smith, J.E. Karp, Final results of a randomized multicenter phase II study of alvocidib, cytarabine, and mitoxantrone versus cytarabine and daunorubicin (7 + 3) in newly diagnosed high-risk acute myeloid leukemia (AML), Leuk. Res. 72 (2018) 92–95, https://doi.org/10.1016/j.leukres.2018.08.005.
[60] C. Pinto, H. Cidade, M. Pinto, M.E. Tiritan, Chiral flavonoids as antitumor agents, Pharmaceuticals 14 (2021) 1267, https://doi.org/10.3390/ph14121267.
[61] Â. Bisol, P.S. de Campos, M.L. Lamers, Flavonoids as anticancer therapies: a systematic review of clinical trials, Phytother. Res. 34 (2020) 568–582, https://doi.org/10.1002/ptr.6551.